Sensors and Actuators A 273 (2018) 90–97

Contents lists available at ScienceDirect

Sensors and Actuators A: Physical

journal homepage: www.elsevier.com/locate/sna

Effect of piezoelectric layer thickness and poling conditions on the performance of cantilever piezoelectric energy harvesters on Ni foils

Hong Goo Yeo[a,b,*], Susan Trolier-McKinstry[a]

[a] Materials Research Institute, The Pennsylvania State University, University Park, PA, 16802, USA
[b] DGIST-ETH Microrobotics Research Center, Daegu-Gyeongbuk Institute of Science and Technology (DGIST), Daegu, 42988, South Korea

ARTICLE INFO

Article history:
Received 17 September 2017
Received in revised form 24 January 2018
Accepted 14 February 2018
Available online 15 February 2018

Keywords:
Piezoelectric thin films
Vibrational energy harvesting
Metal substrate

ABSTRACT

Lead zirconate titanate (PZT) films grown on flexible Ni foils were utilized to explore the effects of thickness and poling conditions on the performance of mechanical energy harvesters. In the case of Mn doped 1 μm thick (001) oriented sol-gel PZT (52/48) films on Ni foil, the dielectric constant and $|e_{31,f}|$ are 390 at 10 kHz and 11.3 C/m^2, respectively, after hot poling. This film has a large figure of merit ($\frac{e^2_{31,f}}{\varepsilon_r}$), of around 0.4 C^2/m^4, for piezoelectric energy harvesting. Unimorph cantilever beams were easily fabricated from PZT films on Ni foil using simple mechanical cutting. The maximum power increases from 12 to 60 μW as the thickness of Nb doped PZT film increases from 1 to 3 μm at resonance frequency (~70 Hz) at 0.5 G. The optimum poling condition (150 °C, at 3 times the coercive for 15 min) enhanced the voltage and power output of the cantilever harvester prepared using (1 μm) PZT films on Ni foil. It was found that the power performance of harvesters strongly depends on the thickness of the film with resonant harvesters of the same footprint area (0.385 cm^2) using PZT films on Ni foils.

1. Introduction

Solar, thermal, and mechanical environmental sources contain energy that is potentially available to harness for the operation of electronics. Energy harvesting technologies which generate electrical power from mechanical vibration or movement for low-power electronic devices (*e.g.* for wireless sensor networks or consumer electronics) are of especial interest when solar energy is unavailable. In principle, mechanical harvesting provides a potential solution to minimize the replacement of batteries for emplaced sensors in remote areas [1]. Lead zirconate titanate (PZT) thin films, which have a high piezoelectric response, are good candidates for piezoelectric microelectromechanical (MEMS) energy harvesters used in scavenging energy from continuous mechanical vibrations. However, high resonant frequencies (typically more than 1 kHz) and low output power are the main challenges for MEMS energy harvesters. The low powers are often a result of a small piezoelectric area combined with stiff a support layer having low fracture toughness [2].

Numerous reports have focused on improving the power density of energy harvesters through advanced device structures, improved circuits for energy extraction, and increased piezoelectric properties [3–8]. To enhance the efficiency of energy transformation from mechanical to electrical energy, it is crucial to optimize the material properties. Improvements in the materials used in piezoelectric energy harvesters (PEH) include the control of composition, crystallographic orientation [9], stress state [8], processing-induced defects (*e.g.* through the preparation of gradient free films) [10], doping [11], and development of strong levels of imprint. Of these, dopants (*e.g.* acceptor and donor) are well known to tailor the properties of PZT film [8,12–14]. For example, Nb^{5+} is a donor dopant that increases the dielectric constant and piezoelectric responses by enhancing domain wall motion [12,13]. In contrast, acceptor dopants such as Mn^{3+} has been reported to lower dielectric constant and loss tangent due to the presence of an internal bias field [8,14].

The maximum extractable electric power for a cantilever structure (Fig. 1) operating in the 31 mode (*e.g.* a piezoelectric layer with top and bottom electrodes, poled out of the plane of the film) is generated at the resonance frequency. The power can be expressed by [15–17]

$$Power_{max} = \frac{m}{4\omega}\left(\frac{e^2_{31,f}}{\varepsilon_r\varepsilon_0}\cdot\frac{(1-\nu_s)^2}{Y_s}\right)Q^2_{tot}A^2 \quad (1)$$

where m is the mass of the proof mass, ω is the natural frequency, ν_s and Y_s are Poisson's ratio and Young's modulus of the passive layer for thin film piezoelectric, $e_{31,f}$ is the piezoelectric

* Corresponding author at: DGOST-ETH Microrobotics Research Center, Daegu-Gyeongbuk Institute of Science & Technology (DGIST), Daegu, 42988, South Korea.
E-mail address: hgyeo@dgist.ac.kr (H.G. Yeo).

https://doi.org/10.1016/j.sna.2018.02.019
0924-4247/

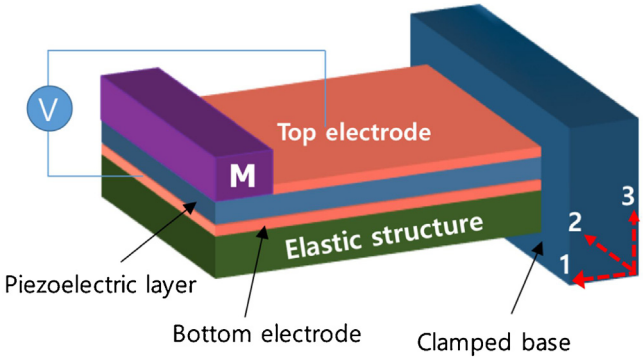

Fig. 1. Illustration of cantilever structure with elastic layer and proof mass (M) for a piezoelectric energy harvester operating in the 31 mode.

coefficient, ε_0 and ε_r are the permittivity of free space and relative permittivity, respectively, Q_{tot} is the total quality factor of the resonating device, and A is the acceleration level. Of these parameters, the transverse coefficient ($e_{31,f}$) and the relative permittivity (ε_r) of the piezoelectric can be modified to increase the energy harvesting figure of merit (FoM), defined as $(e_{31,f})^2/\varepsilon_r$. Therefore, $e_{31,f}$ and ε_r are the crucial materials-based parameters to enhance the output power of piezoelectric energy harvesting MEMS. However, there are few reports that directly demonstrate a link between the figure of merit and the performance of piezoelectric energy harvester for devices of the same size and resonance frequency [18].

In general, the process of poling, where a high DC electric field is applied to the film along the desired direction, is essential to improve the piezoelectric response by alignment of ferroelectric domains in the direction of the applied field [19]. Additionally, the dielectric constant depends on the poled domain state; this is important in controlling the FoM of the energy harvester [20]. Thus, the first goal of this work is to prove the link between the output power of the harvester and the figure of merit; this was done by the use of poling conditions to affect the degree of domain alignment. Even though numerous studies have been reported for fabrication of MEMS piezoelectric energy harvesters, there are few reports that detail how the poling process impacts the performance of MEMS harvesters.

Generally, it is well known that the thickness of the piezoelectric layer is intimately correlated with the harvester performance. While theoretically the relationship between the thickness or volume of piezoelectric material is obvious, it is useful to experimentally validate the relationship using resonant harvesters of the same footprint measured under the same conditions (*e.g* acceleration level, poling) [21]. The second goal of this work is to demonstrate an increase in the extracted voltage for a fixed vibrational input via an increase in the piezoelectric film thickness. For a 31 mode energy harvester, the open circuit voltage V by [16,22]:

$$V = -\frac{e_{31,f}}{\varepsilon_0 \varepsilon_r}(1-\upsilon_s)^2 \frac{3h_s t_p (l_s + l_m)}{l_s^2(4l_s + 3l_m)}\delta_s \quad (2)$$

where t_p, l_s, l_m are the thickness of the PZT thin film, the length of the beam and tip mass, δ_s is cantilever displacement at the boundary between the beam and tip mass, and υ_s is Poisson's ratio of the substrate. Thus, a 31 mode device will generate higher open-circuit voltages when the thickness of the PZT film is increased, provided that the dimensions are fixed (*i.e.* $V \propto t_p$) and the strain is the same. However, it is important to note that the properties of films are rarely constant as a function of thickness [23–25]. In particular, the thick films of interest for mechanical energy harvesting are more susceptible to cracking at high strain levels [26,27]. Such cracking can reduce the $e_{31,f}$ coefficient to zero. Thus, it is important to assess the maximum in the harvester performance as a function of the film thickness.

Table 1
Sputtering and *ex-situ* crystallization conditions of PZT films on $LaNiO_3$//HfO_2//Ni.

Sputtering method	RF-magnetron sputtering
Target	PZT (52/48) + 8% excess PbO + 1% Nb
RF Power	88 W
Chamber Pressure	2 mTorr
Gas	Ar only
Substrate Temperature	Room Temp.
Time	12,500 s for ~0.5 μm
Crystallization Temperature	650 °C in air atmosphere

In this study, highly {001} oriented PZT films with high energy harvesting figures of merit [16] were coated on flexible nickel metal foils. Ni foils can deform plastically, and so are less susceptible to brittle mechanical failure compared to substrates such as Si. In order to assess the importance of PZT film thickness and porosity on the energy harvesting figure of merit and the extracted energy from a vibrational input, piezoelectric MEMS energy harvesters were prepared as rectangular cantilevers 7 mm × 5.5 mm ~0.385 cm^2 with 0.4 g proof mass; thus, all devices had approximately the same resonance frequency (<100 Hz).

2. Device fabrication and measurement

2.1. Fabrication of piezoelectric energy harvesters

{001} oriented Nb or Mn doped PZT thin films were coated on (100)$LaNiO_3$//HfO_2//Ni foils by either *rf*-magnetron sputtering (using a Kurt J. Lesker CMS-18 tool) or chemical solution deposition (CSD).

Prior to growing the piezoelectric layer, a $LaNiO_3$ seed layer and a HfO_2 passivation layer were deposited on 25 μm thick Ni foils (Aldrich Aesar 99.99%) following polishing and pre-annealing as described elsewhere [20]. In brief, atomic layer deposition (ALD, Cambridge Nanotech Savannah 200 ALD System) was used to deposit a 30 nm thick layer of amorphous HfO_2 which is an excellent physical barrier between the Ni foil and atmospheric oxygen at high temperature [28]. (100) oriented $LaNiO_3$ (LNO) was deposited by chemical solution deposition using a 0.2 M $LaNiO_3$ precursor solution based on 2-methoxyethanol (2MOE). Use of these two layers allowed PZT layers to be deposited and crystallized under the same conditions employed to grow PZT films on platinum-coated Si substrates.

Two different approaches were used to grow the PZT films: chemical solution deposition and *rf* magnetron sputtering. 1% Mn doped $Pb(Zr_{0.52}Ti_{0.48})O_3$ films were prepared by CSD using 0.4 M 1% Mn doped PZT solution with 10 mol% excess PbO on $LaNiO_3$//HfO_2//Ni; further details are described in previous work [20]. After all of the spin-coated multiple PZT layers were crystallized, PbO solution was spin coated and crystallized to convert a small amount of lead-deficient phases on the surface to phase-pure perovskite PZT phase. Finally, the Mn doped PZT film had a thickness near 1 μm.

In a second approach, RF magnetron sputtering with *ex situ* post annealing was used to grow PZT films with thicknesses between 1 and 3 μm on (100)LNO//HfO_2//Ni foil using a 1% Nb doped $Pb_{1.08}(Zr_{0.52}Ti_{0.48})O_3$ target under the conditions shown in Table 1. For *rf*-sputtering at room temperature, *ex-situ* crystallization in a rapid thermal annealer was used to crystallize the amorphous PZT layer. Each 0.5 μm layer of PZT was deposited and post annealed to achieve (001) orientation by controlling nucleation at the bottom interface; these layers were stacked until the desired thickness of PZT was achieved as described elsewhere [5]. It was found that

crystallization was required approximately every 0.5 μm in order to retain orientation for the whole film thickness.

X-ray diffraction (XRD, PANalytical X'pert) was used to determine the crystallinity, phase purity, and the orientation of the films. The existence of pores and second phases was assessed through field emission scanning electron microscopy (FE-SEM, Leo 1530, and Merlin) of both cross-sections and the film surface. The electrical properties of all PZT samples were measured using small Pt top electrodes (diameter 200 μm–400 μm). An LCR meter was used for measurement of the dielectric constant and loss as a function of frequency (100 Hz–1 MHz) at low electric field (30 mV). Polarization as a function of electric field was assessed using a Radiant Technologies Precision Multiferroics tester.

For the fabrication of the cantilever piezoelectric energy harvester, 100 nm thick Pt top electrodes (2 mm (length) × 6 mm (width)) were deposited on the PZT film by dc magnetron sputtering (Kurt J. Lesker CMS-18) and patterned using a lift-off process. Additionally, the adhesion strength between the top electrode and the PZT film was enhanced by heat treatment at 500 °C in air. The PZT-coated Ni foils were cut by scissors for fixed-free cantilever beams; most piezoelectric MEMS energy harvesters on silicon substrates require a complex etching process. The PZT beam was 7 mm in width, which is a little larger than the electrode size, to avoid the propagation of cutting-induced cracks into the active area (See FESEM images in Fig. 2). The beams were 5.5 mm in length to provide an area to attach the proof mass.

The PZT beams were poled under various conditions (*e.g.* unpoled, poled at 3 times the coercive field (E_c) at room temperature, or poled at $3E_c$ at 150 °C) to determine the relationship between the transverse piezoelectric coefficient $e_{31,f}$ and the electrical output power from a unimorph PZT beam. The Ni substrate was exposed by scratching the PZT films using a razor blade; this allowed the bottom electrode to be probed. A positive voltage was applied to the bottom electrode for poling. After attaching a brass proof mass (~0.4 g) to the end of the beam, the base of the beam was bonded to a rigid plastic fixture frame. This allowed the harvester to be handled easily and mounted on a shaker with a magnet.

2.2. Experimental setup for testing harvesters

Fig. 3 provides a schematic illustration of the experimental setup for measuring the performance of the vibrational energy harvester. The harvester is shown connected to the external load resistance.

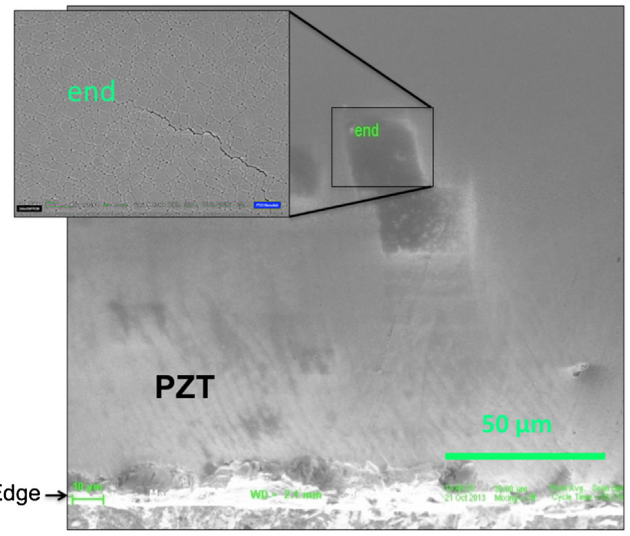

Fig. 2. FESEM surface images of PZT films with cracks near the edge following cutting by scissors.

A shaker table (F3, Wilcoxon) was used as a vibration source. The sinusoidal excitation frequency and base excitation level was controlled using a lock-in-amplifier (SRS830, Stanford Research Systems).

An accelerometer (352C65, PCB Piezotronics) was mounted to the spindle of the shaker to detect the vibration frequency and acceleration level. A magnet, placed on the accelerometer, was utilized to hold the harvesters to the accelerometer. A resistor box connected to the harvester was used to alter the load resistance to determine the optimum value showing maximum output power. During vibration of the shaker, the mechanical input (operating frequency and excitation level) and the output voltage developed by the harvester were monitored on an oscilloscope (TDS3054C, Tekrtronix). The output power was calculated from $P = V^2/R$. Data were taken at multiple frequencies to assess the resonance frequency and the optimal load resistance.

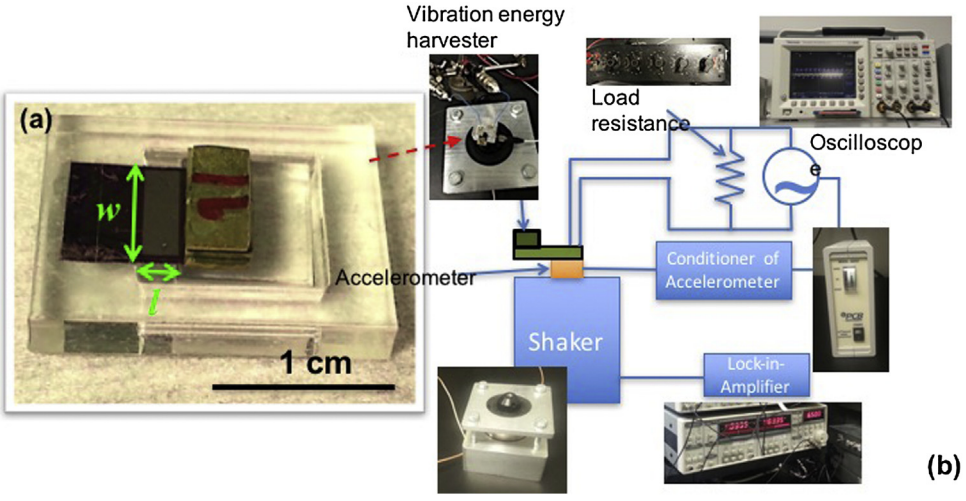

Fig. 3. (a) Top view photograph of a piezoelectric energy harvester utilizing PZT films on Ni foil with a resonance frequency of 63–72 Hz. (b) Experimental setup for measurement of the output performance of the piezoelectric energy harvester.

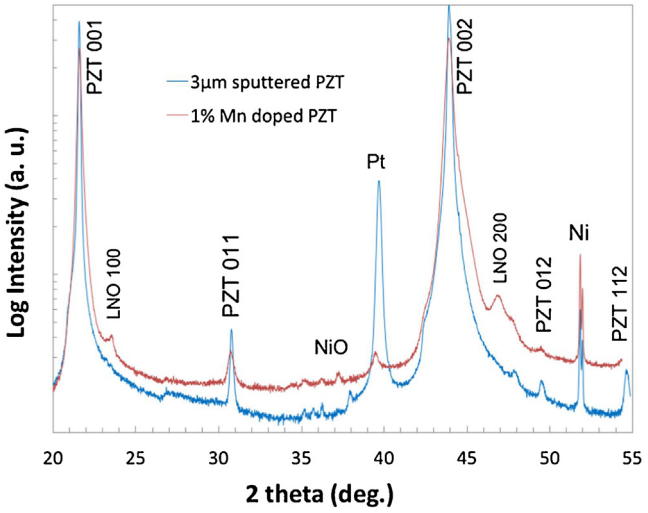

Fig. 4. XRD θ-2θ scan of crystallized PZT (52/48) film grown by sputtering (Nb-doped sample) and CSD (Mn-doped sample) on $LaNiO_3$//HfO_2//Ni.

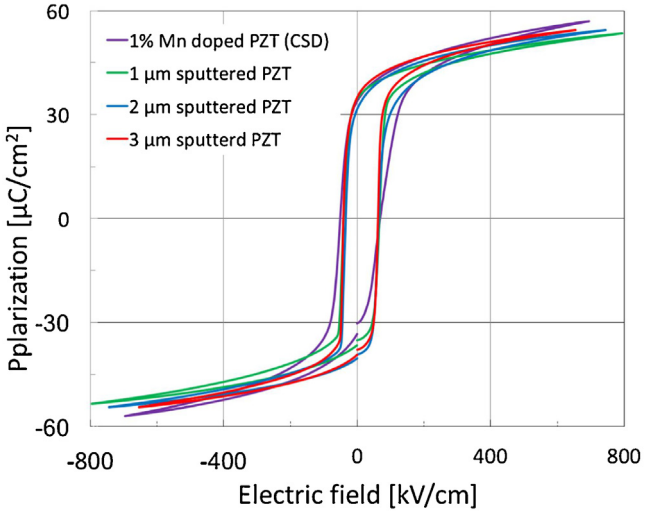

Fig. 6. P–E hysteresis loops of 1–3 μm thick 1% Nb doped sputtered PZT films and 1% Mn doped sol-gel PZT film on Ni foils.

3. Characteristics of thin films and devices

3.1. PZT crystallinity and microstructure

Fig. 4 exhibits the XRD pattern of strongly {001} oriented PZT films on LNO//HfO_2//Ni prepared either by CSD or sputtering with *ex-situ* crystallization. Consistent with the work presented in Ref. [20], strongly {001} oriented PZT films were achieved on Ni foils without a pyrochlore phase by both techniques. In the case of sputtered PZT films, the multilayer stacking with post annealing every 0.5 μm thick layer enables control of the nucleation sites and growth of the desired orientation. $LaNiO_3$ serves as an orienting perovskite seed layer [5]. The crystallinity of the Mn doped PZT film by CSD shows the same results as Nb doped PZT films on Ni foil [20].

Fig. 5(a), (b) show surface and cross section microstructures of the sputtered PZT and sol-gel PZT films. There is no evidence of pyrochlore phase on PZT films grown by either method. In the case of sputtered 1% Nb doped PZT film, a columnar PZT structure with nanoporosity is plainly shown in Fig. 5(a). These pores influence the ferroelectric and piezoelectric properties [29]. On the other hand, the 1% Mn doped PZT (52/48) CSD films have dense and columnar grains [20].

Figs. 6 and 7 show the P–E hysteresis loops and dielectric properties of various thickness PZT films grown by either sputtering or CSD. With 200 μm diameter Pt electrodes, all of the 100 Hz, polarization-electric field hysteresis loops display well-saturated, square hysteresis loops with large remanent polarization ($P_r \sim 40\ \mu C/cm^2$) [5,22]. There is no significant difference between the various specimens as shown in Fig. 6.

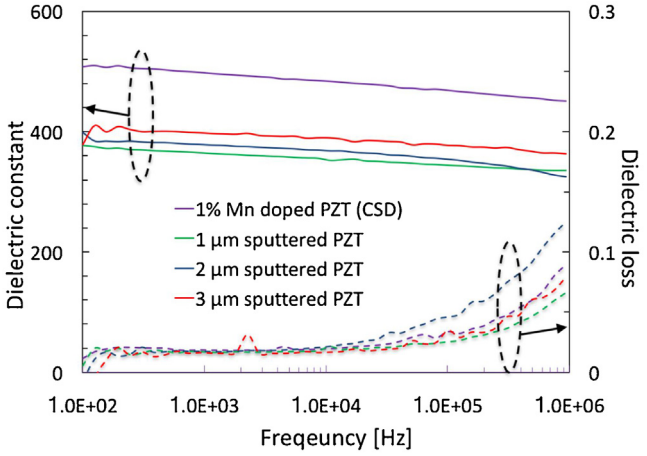

Fig. 7. Dielectric constant and loss of 1–3 μm thick 1% Nb doped sputtered PZT films and 1% Mn doped sol-gel (1 μm) PZT film on Ni foils respectively.

To confirm the material figure of merit for piezoelectric energy harvesters, measurements of the piezoelectric $e_{31,f}$ coefficient and the dielectric constant (ε_r) are essential to directly compare with the power generation from a unimorph cantilever made from the

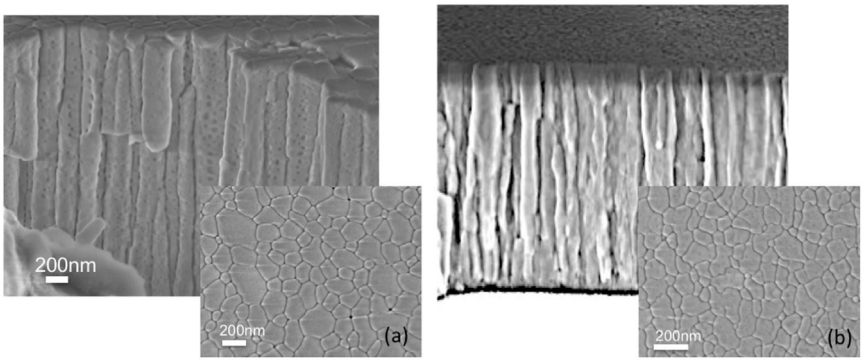

Fig. 5. Comparison of surface FE-SEM image of PZT//LNO//HfO2//Ni cross-sections of PZT films deposited by (a) sputtering and (b) CSD.

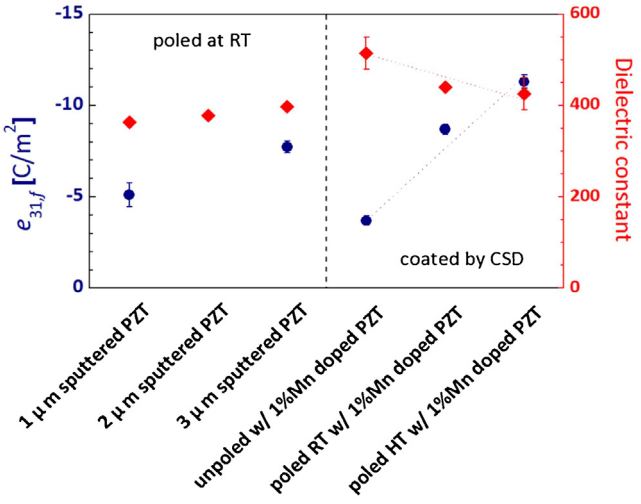

Fig. 8. Transverse piezoelectric coefficient and dielectric constant as a function of thickness, and poling condition [blue circle ($e_{31,f}$), red diamond (dielectric constant)]. (For interpretation of the references to colour in this figure legend, the reader is referred to the web version of this article.)

same piece of PZT film. The dielectric properties measured at a 30 mV oscillation level for all samples after P–E measurement with high electric field (~800 kV/cm) are shown in Fig. 7. Dielectric constants for the sputtered Nb doped PZT films and Mn doped PZT film by CSD were 390 and 500 respectively with a loss tangent of 3% at 10 kHz. The comparatively low relative permittivities are a result of a large *c*-domain population caused by a combination of the crystallographic orientation and compressive stress in the PZT film on cooling [22]. Furthermore, the ε_r of sputtered Nb doped PZT films are lower than that of Mn doped PZT film by CSD. This is a consequence of the porosity in the sputtered films. In principle, Nb doping induces a modest enhancement of dielectric permittivity [13]. However, in the case of our films, the impact of doping on the dielectric permittivity of the PZT films is small compared to the role of porosity (since for air $\varepsilon_r \sim 1$) [30].

In general, the poling conditions influence how well the dipoles are oriented in the allowable direction closest to the direction of applied field, and how stable the net polarization is after removing the applied field [19]. The stability of oriented dipoles is impacted by the build-up of an internal bias field after poling. It is well known that PZT ceramics undergo extensive 180° and non-180° domain switching on poling. PZT films are at least partially mechanically clamped by the substrate and so tend to demonstrate more limited ferroelastic reorientation [29].

The $e_{31,f}$ of various samples were determined by the wafer flexure method [31]. To measure the piezoelectric response of PZT films, the sputtered Nb doped PZT films were poled at 3 times the coercive field for 10 min at room temperature (RT), while Mn doped PZT films by CSD were measured either unpoled, poled at RT, or hot poled at 150 °C. Fig. 8 exhibits the results of $e_{31,f}$ obtained from different thicknesses of sputtered Nb doped PZT films and various poling conditions of sol-gel Mn doped PZT film. In this study, the Nb doping does not significantly affect the piezoelectric response.

For the 1% Mn doped sol-gel PZT films on Ni foil, the dependence of the piezoelectric transverse coefficient on the poling process was assessed. Fig. 8 shows that hot poled films have higher $e_{31,f}$ than either unpoled films or those poled at room temperature. It is believed that the elevated temperatures enhanced the dipole alignment and the stabilization of the domain structure [19]. The higher $e_{31,f}$ produced by hot poling improves the efficiency of piezoelectric energy harvesters [18].

3.2. Performance of harvester dependence on thickness of film

To demonstrate the use of PZT films with strong out-of-plane polarization in a vibrational energy harvesting system, 31 mode cantilever beams were fabricated using strongly {001} textured 1–3 μm thick sputtered Nb doped and 1 μm thick sol-gel Mn doped PZT films on Ni foils. Fig. 3(a) shows a fabricated energy harvesting device with a 0.4 g brass proof mass. The top electrode area is 0.122 cm^2 (2 mm (*l*, length) × 6 mm (*w*, width)). The active area of the fabricated energy harvester, including the proof mass, is around 0.385 cm^2. The resonance frequency of each device was found by sweeping the input frequency for the shaker, and detecting the open circuit voltage on an oscilloscope. At the resonance frequency, the device was excited at an acceleration level of 1.0 G (G = 9.8 m/s^2). The maximum voltages ($V_{max} = V_{pk\text{-}pk}/2$) of 1 μm and 3 μm sputtered 1% Nb doped PZT film were measured to determine the optimum load resistance for maximum power transfer ($P_{max} = V_{max}^2/R$) as shown in Fig. 9(a). The maximized output power of 1 μm and 3 μm thick sputtered PZT films on Ni foil was generated at the optimal load resistance of 50 kΩ and 100 kΩ respectively. In this experiment, the open circuit voltage of devices with 3 μm thick sputtered PZT film is approximately 3.5 times higher than that with 1 μm thick sputtered PZT film at the same excitation level. The slight discrepancy between theoretical and experiment values was caused by small fabrication-induced differences in dimension or tip displacement. Thus, the results support experimentally the relationship between the thickness of the PZT film and the open circuit output voltage.

At the optimal load resistance, the maximum output power depends on frequency as shown in Fig. 9(b). The sample with 1 μm thick sputtered PZT film has a resonance frequency of 69 Hz. Most of the devices prepared in this work have similar resonance frequencies (around 65 Hz) with slight deviations mainly caused by small differences of dimension. The variation is small enough to enable direct comparison. The mechanical quality factor (Q) and mechanical damping ratio (ζ) also have strong roles in controlling the achievable output power. In this work, Q was defined using the half power method as: $Q = f_r/(f_b - f_a)$ where f_r is the resonance frequency and the bandwidth at the half-maximum amplitude (FWHM) is $f_b - f_a$ [32,33]. High Q-factors of a device indicate high power sensitivity as function of frequency; *i.e.* a narrow frequency bandwidth leads to a tremendous drop of the output power if the input vibration frequency deviates from the resonance frequency of the device. On the other hand, a lower Q-factor with a broad frequency bandwidth is suitable for increasing scavenged energy from a wide spectrum of environmental vibration [34]. The mechanical quality factor of all samples was around 13.9 ± 1.3. The mechanical damping ratio ($\zeta = (f_b - f_a)/2f_r$) was 3.6% in Fig. 9(b). The Q value is lower than the previous reported Q values of (233) PZT on Si, (85) transferred PZT to stainless steel PZT, and (30) KNN on metal foil [2,32,34].

Fig. 9(c) exhibits the maximum output power as a function of acceleration level for samples with 1–3 μm thick sputtered PZT films. Overall, the output power increases rapidly with acceleration level below 0.5 G acceleration and then rises more slowly. Ideally, the output power is proportional to the square of the acceleration level (A) per Eq. (1). However, an increase of air damping and nonlinear elastic compliance at large stresses (large acceleration levels) can provide lower power densities as a function of acceleration level [34,35].

3.3. Performance of harvester dependence on poling condition

As mentioned earlier, improvement of FoM of piezoelectric materials depends on the poling condition such as electric field, time and temperature. Thus, the poling efficiency strongly impacts

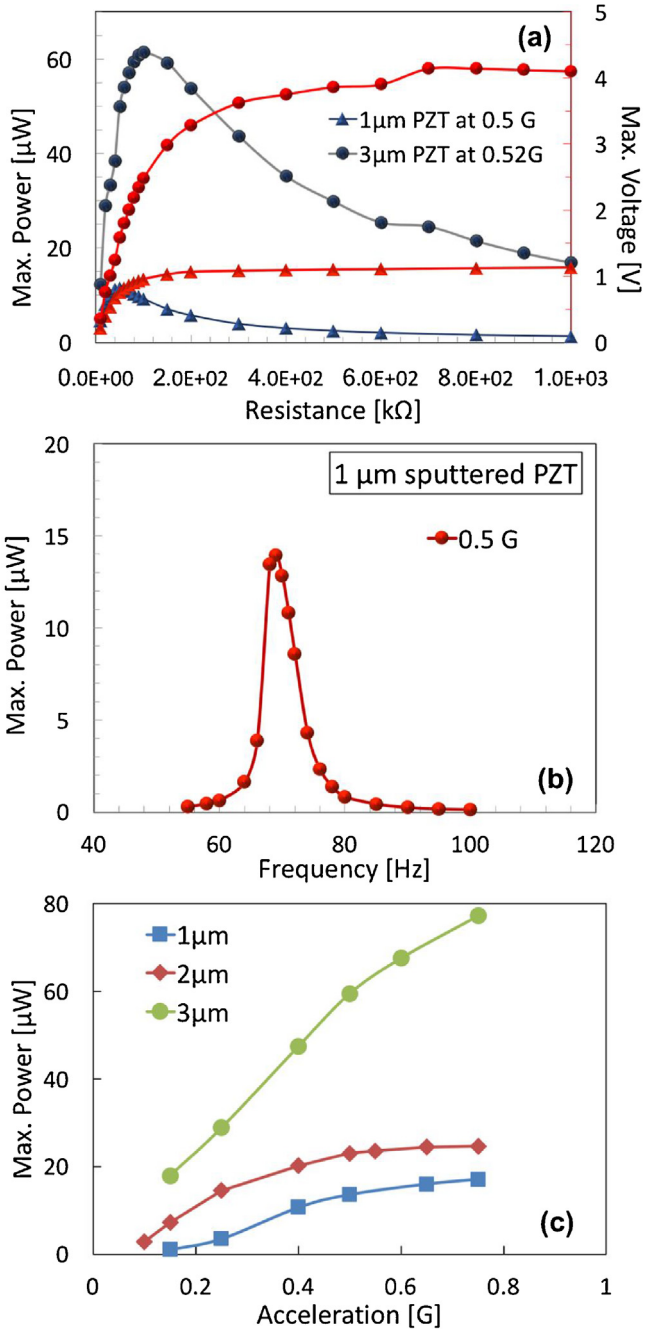

Fig. 9. Maximum output power as a function of (a) external load resistance, (b) frequency at 0.5 G, and (c) Maximum output power as a function acceleration level with optimum load resistance of piezoelectric energy harvester using 1–3 μm thick (001) oriented 1% Nb doped sputtered PZT films on Ni foil (25 μm) measured at resonance.

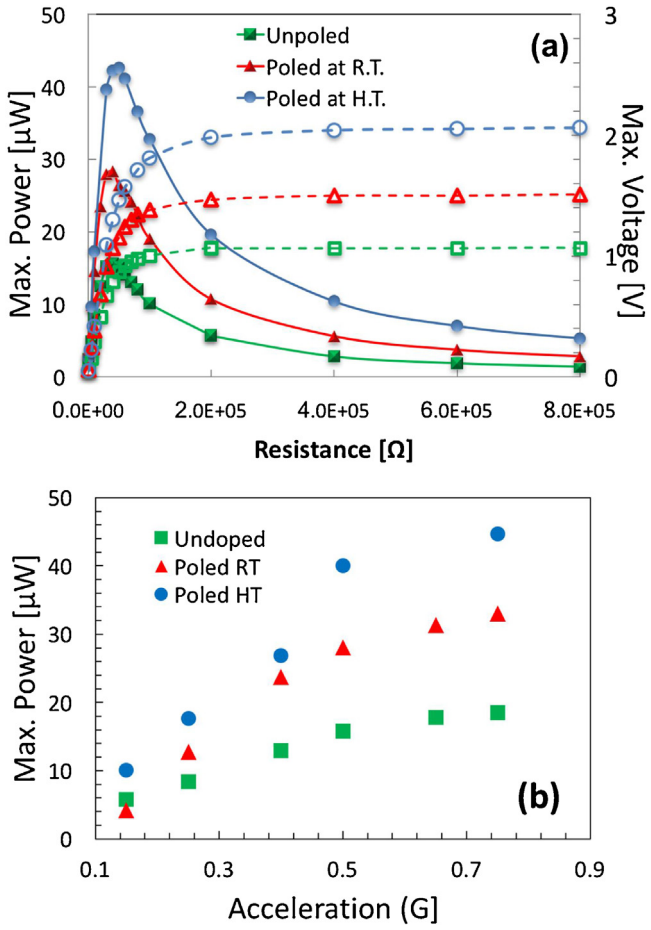

Fig. 10. Maximum output (bold) power as a function of (a) external load resistance at 0.5 G and (b) acceleration level at optimum load resistance of piezoelectric energy harvester using 1 μm thick 1% Mn doped sol-gel PZT films on Ni foil at resonance.

the output of the piezoelectric harvester [18]. Using Mn doped sol-gel PZT films on Ni foil, the output voltage was measured for different poling conditions. Fig. 10 exhibits the output voltage and generated power as a function of external load resistance for samples that are unpoled, poled at room temperature (RT) and poled at 150 °C (high temperature (HT)). For the same acceleration level (0.5 G) and frequency, it is observed that the hot poling process improves the extracted power compared with the performance of either unpoled or RT poled samples, due to more efficient domain alignment [18].

The optimum load resistance of unpoled and RT poled samples was about 40 kΩ. On the other hand, the optimum load resistance was 50 kΩ after hot poling. This is because the electrical load resistance matching depends on the capacitance of the device [32]. Hot poling reduced the dielectric constant of the PZT film due to significant preferential *c*-domain alignment, the development of imprint, and possibly reduction in the domain wall density. Fig. 10(b) shows the output power of a harvester as a function of acceleration amplitude using 1 mol% Mn doped sol-gel PZT films under different poling conditions. Based on Eq. (2), if the excitation is constant for a given total (electrical and mechanical) quality factor, the power is proportional to the FoM. Because the dielectric loss tangents (and hence the electrical quality factor) of the films were all comparable, the data in Table 2 show reasonable proportionality between the generated electrical power and the FoM.

Overall, the hot poling process delivers better output performance than either unpoled or room temperature poled samples as shown in Fig. 10(b). Thus, enhanced piezoelectric response and reduction of permittivity from the poling improved the generated power from the cantilever harvester [18]. Similar trends were observed using sputtered 1% Nb doped PZT films on Ni foil in Fig. 9(c).

For both deposition methods, at increased acceleration level, the power does not rise as fast as predicted, presumably due to the enhancement of mechanical damping [2].

Table 2 shows the relationship between piezoelectric, dielectric properties and output performance of PZT films on Ni foil based on the results of this work. 3 μm thick sputtered films on Ni foil shows better output performance compared with thinner PZT films, even if they have similar piezoelectric and electrical properties. Thus,

Table 2
Summary of the performance of sputtered and sol-gel PZT films on Ni foils.

Thickness of PZT film	Poling condition	FoM	Res. Freq. @ 0.5 G [1G ≈ 9.8 m/s^2]	Max. Voltage [mV]	Optimal Load Resistance [kΩ]	Max. Power [μW]
1 μm (Sputtered)	3 × E_C at R.T	0.071	69	760	50	12
2 μm (Sputtered)			62	1190	70	23
3 μm (Sputtered)		0.15	72	2440	100	60
1% Mn doping PZT 1 μm (CSD)	No poling	0.026	63	790	40	15.6
	Poling at RT	0.17	63	1065	40	28
	Poling at 150 °C	0.33	63	1460	50	42.6

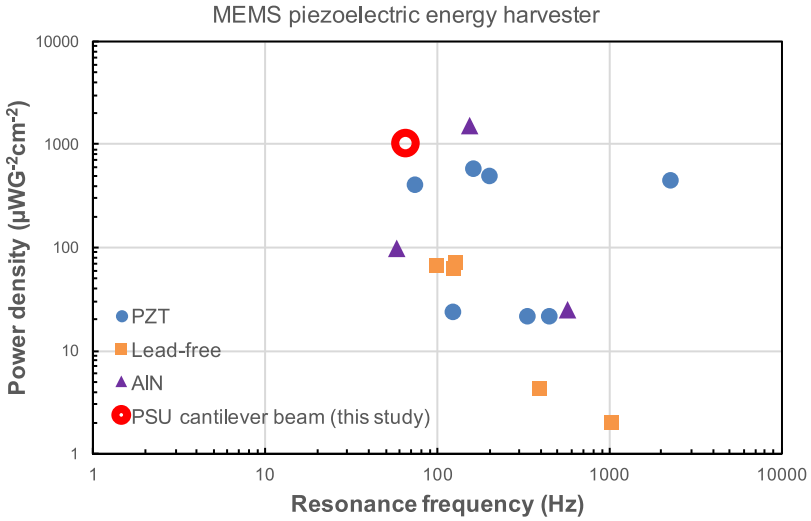

Fig. 11. Power density and resonance frequency of MEMS piezoelectric energy harvesters for a variety of piezoelectric materials reported; PZT [2,34,38–42], Lead-free (KNN [32,35,43,44], and $BiFeO_3$ [45]), AlN [46–48].

there is an incentive to grow thicker films for harvesting. The result is consistent with the simulation developed by Xue and Roundy in terms of relation between average power and the ratio of piezoelectric films (t_{PZT}) to total beam thickness (t_{total}) [36]. The simulation based on Erturk and Inman's distributed bimorph beam model under base excitation demonstrates that the average power is significantly increased by increasing the ratio of thickness (t_{PZT}/t_{total}) from 0 to 0.4 [37].

Fig. 11 exhibits the power density and resonance frequency of several MEMS piezoelectric cantilevers energy harvesters reported in the literature [2,32,35,38–48]. The performance ($Power_{rms}$ = 9 μW at 0.15 G) of the device with 3 μm sputtered PZT thin films investigated in the study is indicated with a red circle. As seen in Fig. 11, the harvester developed in this work possesses some of the highest power densities (1036 μW/cm^2 G^2) measured at low frequency (<100 Hz) reported in the literature.

4. Conclusions

In summary, piezoelectric energy harvesters using oriented PZT films grown either by sputtering or CSD were successfully fabricated with similar dimensions to determine the relationship between output power performance, PZT thickness, and piezoelectric response. It was found that the volume of the PZT layer strongly depended upon the power output of the devices under the same conditions. All devices operated around 68 Hz. Piezoelectric energy harvesters with 3 μm thick sputtered 1% Nb doped PZT film on Ni resulted in an average power density of 1036 μW/cm^2 G^2. An enhanced power density of the harvester (582 μW/cm^2 G^2) was achieved using an elevated temperature poling process, with 1% Mn doped sol-gel PZT films on Ni foil, relative to room temperature poling. This result promises the extraction of energy from ambient vibration with high power density for use in devices consuming energy in microwatt ranges.

Acknowledgements

This work was supported by a National Security Science and Engineering faculty fellowship and the NSF ASSIST ERC (EEC-1160483).

References

[1] C.R. Bowen, H.A. Kim, P.M. Weaver, S. Dunn, Piezoelectric and ferroelectric materials and structures for energy harvesting applications, Energy Environ. Sci. 7 (1) (2014) 25–44.
[2] K. Morimot, I. Kanno, K. Wasa, H. Kotera, High-efficiency piezoelectric energy harvesters of c-axis-oriented epitaxial PZT films transferred onto stainless steel cantilevers, Sens. Actuators A: Phys. 163 (2010) 428–432.
[3] S.-G. Kim, S. Priya, I. Kanno, Piezoelectric MEMS for energy harvesting, MRS Bull. 37 (2012) 1039–1050.
[4] A. Hajati, S.G. Kim, Ultra-wide bandwidth piezoelectric energy harvesting, Appl. Phys. Lett. 99 (8) (2011) 083105.
[5] H.G. Yeo, X. Ma, C. Rahn, S. Trolier-McKinstry, Efficient piezoelectric energy harvesters utilizing (001) textured bimorph PZT films on flexible metal foils, Adv. Funct. Mater. 26 (32) (2016) 5940–5946.
[6] L. Dhakar, H. Liu, F.E.H. Tay, C. Lee, A new energy harvester design for high power output at low frequencies, Sens. Actuators A 199 (2013) 344–352.
[7] S. Roundy, P.K. Wright, A piezoelectric vibration based generator for wireless electronics, Smart Mater. Struct. 13 (5) (2004) 1131–1142.
[8] C.B. Yeager, S. Trolier-McKinstry, Epitaxial $Pb(Zr_x,Ti_{1-x})O_3$ ($0.30 \leq x \leq 0.63$) films on (100)MgO substrates for energy harvesting applications, J. Appl. Phys. 112 (7) (2012) 074107.
[9] N. Lederman, P. Muralt, J. Baborowski, S. Gentil, K. Mukati, M. Cantoni, A. Seifert, N. Setter, {100}-Textured, piezoelectric Pb(Zr, Ti)O_3 thin films for MEMS: integration, deposition and properties, Sens. Actuators A 105 (2) (2003) 162–170.
[10] F. Calame, P. Muralt, Growth and properties of gradient free sol-gel lead zirconate titanate thin films, Appl. Phys. Lett. 90 (6) (2007) 062907.
[11] K. Wasa, T. Matsushima, H. Adachi, I. Kanno, H. Kotera, Thin-film piezoelectric materials for a better energy harvesting MEMS, J. Microelectromech. Syst. 12 (2) (2012) 451–457.

[12] T. Haccart, D. Remiens, E. Cattan, Substitution of Nb doping on the structural, microstructural and electrical properties in PZT films, Thin Solid Films 423 (2003) 235–242.
[13] W. Zhu, I. Fujii, W. Ren, S. Trolier-McKinstry, Domain wall motion in A and B site donor-doped Pb(Zr0.$Ti_{0.48}$)O_3 films, J. Am. Ceram. Soc. 95 (2012) 2906–2913.
[14] W. Zhu, I. Fujii, W. Ren, S. Trolier-McKinstry, Influence of Mn doping on domain wall motion in Pb(Zr0.$Ti_{0.48}$)O_3 films, J. Appl. Phys. 109 (2011) 064105.
[15] S. Roundy, On the effectiveness of vibration-based energy harvesting, J. Intell. Mater. Syst. Struct. 16 (10) (2005) 809–823.
[16] T.M. Kamel, R. Elfrink, M. Renaud, D. Hohfeld, M. Goedbloed, C. deNooijer, M. Jambunathan, R. von Schaijk, Modeling and characterization of MEMS-based piezoelectric harvesting devices, J. Micromech. Microeng. 20 (10) (2010) 105023.
[17] M.A. Dubois, P. Muralt, Measurement of the effective transverse piezoelectric coefficient $e_{31,f}$ of AlN and Pb (Zr_x,Ti_{1-x})O_3 thin films, Sens. Actuators A 77 (2) (1999) 106–112.
[18] E.M.A. Fuentes-Fernandez, B.E. Gnade, M.A. Quevedo-Lopez, P. Shah, H.N. Alshareef, The effect of poling conditions on the performance of piezoelectric energy harvesters fabricated by wet chemistry, J. Mater. Chem. A 3 (18) (2015) 9837–9842.
[19] A.L. Kholkin, D.V. Taylor, N. Setter, Poling effect on the piezoelectric properties of lead zirconate titanate thin films, in: ISAF 98, Proceeding of the Eleventh IEEE International Symposium on Applications of Ferroelectrics, Montreux, Switzerland, 1998, pp. 69–72.
[20] H.G. Yeo, S. Trolier-McKinstry, {001} Oriented piezoelectric films prepared by chemical solution deposition on Ni foils, J. Appl. Phys. 116 (1) (2014) 014105.
[21] C.G. Hindrichsen, R. Lou-Møller, K. Hansen, E.V. Thomsen, Advantages of PZT thick film for MEMS sensors, Sens. Actuators A: Phys. 163 (1) (2010) 9–14.
[22] Y. Tsujiura, E. Suwa, F. Kurokawa, H. Hida, I. Kanno, Modeling of metal-based piezoelectric MEMS energy harvesters, in: 2013 International Symposium on Micro-NanoMechatronics and Human Science (MHS), IEEE, 2013, pp. 1–4.
[23] J.F. Shepard Jr., F. Chu, I. Kanno, S. Trolier-McKinstry, Characterization and aging response ofthe d_{31} piezoelectric coefficient of lead zirconate titanate thin films, J. Appl. Phys. 85 (9) (1999) 6711–6716.
[24] P. Bintachitt, Local Origin of Macroscopic Properties and Patterning in $PbZr_{1-x}Ti_xO_3$ Films, Doctoral Dissertation, The Pennsylvania State University, 2009.
[25] H. Daniel Chen, K.R. Udayakumar, Christopher J. Gaskey, L. Eric Cross, Jonathan J. Bernstein, Lance C. Niles, Fabrication and electrical properties of lead zirconate titanate thick films, J. Am. Ceram. Soc. 79 (8) (1996) 2189–2192.
[26] C.S. Park, J.W. Lee, G.T. Park, H.E. Kim, J.J. Choi, Microstructural evolution and piezoelectric properties of thick Pb(Zr,Ti)O_3 films deposited by multi-sputtering method: part I. Microstructural evolution, J. Mater. Res. 22 (05) (2007) 1367–1372.
[27] G.A. Schneider, Influence of electric field and mechanical stresses on the fracture of ferroelectrics, Annu. Rev. Mater. Res. 37 (1) (2007) 491–538.
[28] D.S.B. Heidary, C.A. Randall, Study on the behavior of atomic layer deposition coatings on a nickel substrate at high temperature, Nanotechnology 27 (2016) 245701.
[29] S. Trolier-McKinstry, P. Muralt, Thin films piezoelectric for MEMS, J. Electroceram. 12 (2004) 7–17.
[30] J.I. Roscow, R.W.C. Lwewis, J. Taylor, C.R. Bowen, Modeling and fabrication of porous sandwich layer barium titanate with improved piezoelectric energy harvesting figures of merit, Acta Mater. 128 (2017) 207–217.
[31] R. Wilke, P. Moses, P. Jousse, C. Yeager, S. Trolier-McKinstry, Wafer mapping of the transverse piezoelectric coefficient, e31,f, using the wafer flexure technique with sputter deposited Pt strain gauges, Sens. Actuators A 173 (1) (2012) 152–157.
[32] T. Shiraishi, N. Kaneko, M. Kurosawa, H. Uchida, Y. Suzuki, T. Kobayashi, H. Funakubo, Vibration-energy-harvesting properties of hydrothermally synthesized (K, Na)NbO_3 films deposited on flexible metal foil substrates, Jpn. J. Appl. Phys. 54 (2015) 10ND06.
[33] B. Crowell, Vibrations and Waves, Light and Matter Online Text Series, Ch.2, 2006.
[34] D. Shen, J.-H. Park, J. Ajitsaria, S.-Y. Choe, H.C. Wikel III, D.-J. Kim, The design, fabrication and evaluation of a MEMS PZT cantilever with an integrated Si proof mass for vibration energy harvesting, J. Micromech. Microeng. 18 (2008) 055017.
[35] Y. Tsujiura, E. Suwa, F. Kurokawa, H. Hida, K. Suenaga, K. Shibata, I. Kanno, Lead-free piezoelectric MEMS energy harvesters of (K, Na)NbO_3 thin films on stainless steel cantilevers, Jpn. J. Appl. Phys. 52 (2013) 09KD13.
[36] unpublished data from Tiancheng Xue and Shad Roundy, the University of Utah.
[37] A. Erturk, D.J. Inman, An experimentally validated bimorph cantilever model for piezoelectric energy harvesting from excitations, Smart Mater. Struct. 18 (2) (2009) 025009.
[38] D. Isarakorn, D. Briand, P. Janphuang, A. Sambri, S. Gariglio, J.-M. Triscone, F. Guy, J.W. Reiner, C.H. Ahn, N.F. de Rooij, Energy harvesting MEMS device based on an epitaxial PZT thin film: fabrication and characterization, Power MEMS Tech. Dig. (2010) 203.
[39] E.E. Aktakka, R.L. Rebecca, N. Khalil, Thinned-PZT on SOI process and design optimization for piezoelectric inertial energy harvesting, in: 16th International Conference on Solid-State Sensors, Actuators, and Microsystems, Transducers, 2011, pp. 1649.
[40] T. Zawada, K. Hansen, R. Lou-Moeller, E. Ringgaard, T. Pedersen, E.V. Thomsen, High-performance piezoelectric thick film based energy harvesting micro-generators for MEMS, Procedia Eng. 5 (2010) 1164–1167.
[41] R. Xu, A. Lei, C. Dahl-Petersen, K. Hansen, M. Guizzetti, K. Birkelund, O. Hansen, Screen printed PZT/PZT thick film bimorph MEMS cantilever device for vibration energy harvesting, Sens. Actuators A: Phys. 188 (2012) 383–388.
[42] H. Durou, G.A. Ardilla-Rodriguez, A. Ramond, X. Dollat, C. Rossi, D. Esteve, Micromachined bulk PZT piezoelectric vibration harvester to improve effectiveness over low amplitude and low frequency vibrations, in: PowerMEMS 2010, Leuven, Belgium, 2010, p. 27.
[43] I. Kanno, T. Ichida, K. Adachi, H. Kotera, K. Shibata, T. Mishima, Power-generation performance of lead-free (K, Na)NbO_3 piezoelectric thin-film energy harvesters, Sens. Actuators A: Phys. 179 (2012) 132–136.
[44] S.-H. Kim, H. Seo, S. Glinsek, Y. Kim, A.I. Kingon, Lead-free piezoelectric thin film-based energy harvesters for self-powered implantable medical devices, in: 16th US-Japan Seminar on Dielectric and Piezoelectric Materials, 2013, pp. D13.
[45] T. Yoshimura, S. Murakami, K. Wakazono, K. Kariya, N. Fujimura, Piezoelectric vibrational energy harvester using lead-free ferroelectric $BiFeO_3$ films, Appl. Phys. Exp. 6 (2013) 051501.
[46] T. Ricart, P.P. Lassagne, S. Boisseau, G. Despesse, A. Lefervre, C. Billard, E. Defay, Macro energy harvester based on aluminium nitride thin films, in: 2011 IEEE International Ultrasonics Symposium, IEEE, 2011, p. 1928.
[47] R. Andosca, T. McDonald, V. Genova, S. Rosenberg, J. Keating, C. Benedixen, J. Wu, Experimental and theoretical studies on MEMS piezoelectric vibrational energy harvesters with mass loading, Sens. Actuators A 178 (2012) 76–87.
[48] R. Elfrink, T.M. Kamel, M. Goedbloed, S. Matova, D. Hohlfeld, Y. Van Andel, R. Van Schaijk, Vibration energy harvesting with aluminum nitride-based piezoelectric devices, J. Micromech. Microeng. 19 (9) (2009) 094005.

Biographies

Hong Goo Yeo completed his Ph. D degree in Department of Materials Science and Engineering at The Pennsylvania State University in 2017. His research focuses on processing and properties of the piezoelectric thin films with flexible metal foil substrates for piezoelectric energy harvesting MEMS devices.

Susan Trolier-McKinstry is the Steward S. Flaschen Professor of Ceramic Science and Engineering, Professor of Electrical Engineering, and Director of the Nanofabrication facility at the Pennsylvania State University. Her main research interests include thin films for dielectric and piezoelectric applications. She is a fellow of the American Ceramic Society, IEEE, and the Materials Research Society, and an academician of the World Academy of Ceramics. She currently serves as an associate editor for *Applied Physics Letters*. She is 2017 President of the Materials Research Society; previously she served as president of the IEEE Ultrasonics, Ferroelectrics and Frequency Control Society, as well as Keramos. Twenty people that she has advised/co-advised have gone on to take faculty positions around the world.